tvst

Article

Retinal Pigment Epithelium Atrophy in Recessive Stargardt Disease as Measured by Short-Wavelength and Near-Infrared Autofluorescence

Ruben Jauregui[1,2], Yan Nuzbrokh[1,2], Pei-Yin Su[1], Jana Zernant[1], Rando Allikmets[1,3], Stephen H. Tsang[1–3], and Janet R. Sparrow[1–3]

[1] Department of Ophthalmology, Edward S. Harkness Eye Institute, Columbia University Medical Center, New York, NY, USA
[2] Jonas Children's Vision Care, New York, NY, USA
[3] Department of Pathology & Cell Biology, Columbia University Medical Center, New York, NY, USA

Correspondence: Janet R. Sparrow, Harkness Eye Institute, Columbia University Medical Center, 635 West 165th Street, Box 212, New York, NY 10032, USA. e-mail: jrs88@cumc.columbia.edu

Received: May 5, 2020
Accepted: November 10, 2020
Published: January 5, 2021

Keywords: Stargardt disease; short-wavelength autofluorescence; near-infrared autofluorescence

Citation: Jauregui R, Nuzbrokh Y, Su P-Y, Zernant J, Allikmets R, Tsang SH, Sparrow JR. Retinal pigment epithelium atrophy in recessive Stargardt disease as measured by short-wavelength and near-infrared autofluorescence. Trans Vis Sci Tech. 2021;10(1):3, https://doi.org/10.1167/tvst.10.1.3

Purpose: To compare the detection of retinal pigment epithelium (RPE) atrophy in short-wavelength (SW-AF) and near-infrared autofluorescence (NIR-AF) images in Stargardt disease (STGD1) patients.

Methods: SW-AF and NIR-AF images (115 eyes from 115 patients) were analyzed by two independent graders. Hypoautofluorescent (hypoAF) areas, indicative of RPE atrophy, were measured, and the two modalities were compared.

Results: Patients were segregated into four groups: nascent (6 [5%]), widespread (21 [18%]), discrete (55 [48%]), and chorioretinal atrophy (33 [29%]). The areas of hypoAF were larger in NIR-AF compared to SW-AF images in discrete (3.9 vs. 2.2 mm^2, $P < 0.001$) and chorioretinal atrophy (12.7 vs. 11.4 mm^2, $P = 0.015$). Similar findings were observed qualitatively in nascent and widespread atrophy patients. Using the area linear model (ALM), lesion area increased at similar rates in SW-AF and NIR-AF images of discrete atrophy (0.20 vs. 0.32 mm^2/y, $P = 0.275$) and chorioretinal atrophy (1.30 vs. 1.74 mm^2/y, $P = 0.671$). Using the radius linear model (RLM), the lesion effective radius also increased similarly in SW-AF and NIR-AF images in discrete (0.03 vs. 0.05 mm^2/y, $P = 0.221$) and chorioretinal atrophy (0.08 vs. 0.10 mm^2/y, $P = 0.754$) patients.

Conclusions: NIR-AF reveals a larger area of RPE atrophy in STGD1 patients compared to SW-AF images, but rates of lesion enlargement in the two modalities are similar.

Translational Relevance: Measurements of RPE atrophy by AF imaging are crucial for monitoring STGD1 disease progression and given our findings we advocate greater use of NIR-AF for patients.

Introduction

Recessive Stargardt disease (STGD1) is the most common form of juvenile macular degeneration and is characterized by a progressive loss of central vision, with onset of symptoms usually occurring during the teenage years.[1,2] In affected individuals, mutations are present in the *ABCA4* gene, which encodes the adenosine triphosphate (ATP)-binding cassette transporter in photoreceptors.[3] When functional, *ABCA4* helps clearing all-*trans*-retinaldehyde and thus attenuates excess accumulation of the toxic bisretinoid fluorophores that constitute the lipofuscin in the retina.[4] Reduced or absent transporter activity as in STGD1 results in more rapid accumulation of lipofuscin in the retinal pigment epithelium (RPE) cells, the end result of which is RPE and photoreceptor cell degeneration.[5–7] Although STGD1 is clinically heterogeneous, macular atrophy and yellow-white flecks in the posterior pole or mid-periphery are often observed on fundoscopic examination.[8,9]

The diagnosis and monitoring of STGD1 in individuals is reliant on noninvasive imaging modalities, including short-wavelength fundus autofluores-

cence (SW-AF) and near-infrared autofluorescence (NIR-AF) imaging. The autofluorescence signal captured in SW-AF images (488 nm excitation) originates primarily from the bisretinoid fluorophores that constitute RPE lipofuscin, with contributions also from photoreceptor cells in diseased states.[10,11] The signal captured by NIR-AF (787 nm excitation) arises from melanin in the RPE with a smaller contribution from the choroid.[12] Albeit with smaller patient cohorts, multiple studies have reported that the areas of RPE atrophy on NIR-AF images exceed those on SW-AF images in STGD1 patients.[13–16] In addition, it has been reported that the larger hypoAF area on NIR-AF images exceeds the region of ellipsoid zone (EZ) band loss, suggesting that RPE cell loss occurs before photoreceptor loss.[13] Previous studies from our group in retinitis pigmentosa have also suggested that NIR-AF images reveal a larger extent of retinal damage compared to SW-AF images.[17,18]

In this study, we analyze a large cohort of genetically confirmed STGD1 patients and compare the measurements of hypoAF areas of RPE atrophy in both SW-AF and NIR-AF images. Furthermore, we also compare the rates of atrophic lesion enlargement on both SW-AF and NIR-AF images and explore the presentation of different phenotypes of STGD1 in these imaging modalities.

Methods

This retrospective longitudinal study followed the tenets of the Declaration of Helsinki. Procedures were defined, and informed patient consent was obtained as detailed by the protocol no. AAAI9906 approved by the Institutional Review Board at Columbia University Medical Center.

Patients

We conducted a retrospective review of patients with a clinical diagnosis of STGD1 confirmed by sequencing of the *ABCA4* gene. The unequivocal diagnosis of STGD1 is established when biallelic variants in the gene *ABCA4* are documented, because retinal disease caused by other genes such as *CRX* and *PRPH2* can phenotypically mimic STGD1.[19] Thus patients with only a single identified possibly pathogenic variant were excluded from this study. The biallelic variants were considered to be pathogenic or likely pathogenic by criteria as per the American College of Medical Genetics and Genomics guidelines for the interpretation of sequence variants.[20] Patients were also included if SW-AF and NIR-AF imaging were performed on the same clinic visit, because it is routine practice in this clinic for STGD1 patients with confirmed diallelic *ABCA4* variants to be imaged with both imaging modalities. Patients with end-stage disease were excluded, because high-quality images could not be obtained.

Clinical Examination and Image Acquisition

Pupils were dilated (>7 mm) with phenylephrine hydrochloride (2.5%) and tropicamide (1%) before imaging. Clinical examination included a slit-lamp and fundoscopic examination, best-corrected visual acuity, spectral-domain optical coherence tomography (SD-OCT) imaging, and short-wavelength (SW-AF, 488 nm excitation) and near-infrared autofluorescence (NIR-AF, 787nm excitation). SW-AF imaging was performed using the Spectralis HRA+OCT (Heidelberg Engineering, Heidelberg, Germany) whereas NIR-AF imaging was performed using the Heidelberg Retina Angiograph 2 scanning laser ophthalmoscope (HRA2-SLO; Heidelberg Engineering) using the indocyanine green angiography mode (without injection of dye).

Image Analyses and Measurements of Lesion Area

A total of 115 patients (115 right eyes) were analyzed for this study by two independent observers (RJ and YN). Because of the heterogeneity of STGD1, patients were stratified into four groups that we defined on the basis of the morphology of the areas of RPE atrophy: (1) nascent atrophy, (2) widespread atrophy, (3) discrete atrophy, and (4) chorioretinal atrophy (Table 1). We defined RPE atrophy as areas of hypoAF signal in SW-AF and NIR-AF images compared to what is observed in healthy subjects. For both the nascent and widespread atrophy groups, the AF images were analyzed qualitatively because the areas of RPE atrophy were either diffuse or not well delineated and thus could not be measured. On the contrary, the discrete and chorioretinal atrophy groups presented with areas of atrophy with clear and well-delineated borders that allowed a quantitative analysis of lesion size to be performed.

The hypoAF areas of patients in the discrete and chorioretinal atrophy groups were measured using the semi-automated software tool RegionFinder (Heidelberg Engineering), similar to other studies.[21,22] Intraobserver and interobserver measurement reproducibility using this software has previously been validated.[23,24] Two authors (RJ and YN) performed these measurements to mitigate bias and error. The

Table 1. Division of Patient Cohort Into Groups Based on the Phenotype of Retinal Pigment Epithelium Atrophy

Morphology of RPE Atrophy	N (%)	Age at Presentation (yrs)	Most Common *ABCA4* Allelic Variant (N, %)
Total	115	33 ± 16	p.G1961E (42, 37%)
Nascent	6 (5)	28 ± 8	p.G1961E (5, 83%)
Widespread	21 (18)	30 ± 16	p.P1380L (6, 29%)
Discrete	55 (48)	26 ± 11	p.G1961E (25, 45%)
Chorioretinal	33 (29)	50 ± 13	p.N1868I (9, 27%)

Data are summarized as mean ± standard deviation where appropriate. N = number of patients; yrs = years.

Pearson correlation was used to analyze the measurement agreement by the two graders (SW-AF: $r = 0.999$, $P < 0.001$; NIR-AF: $r = 0.999$, $P < 0.001$). Bland-Altman analyses were performed to further characterize measurement agreement and reproducibility (Supplementary Fig.). Given the high level of correlation and agreement of the measurements between the two graders, the average of the two values was calculated for each measurement and used for subsequent analyses. A paired Student's *t*-test was used to test for a difference in size of the areas of atrophy as observed in SW-AF versus NIR-AF images.

Calculations of the Rates of Lesion Area Enlargement

For patients in the discrete and chorioretinal atrophy groups with two separate visits, we calculated the rate of lesion area enlargement with two methods. In Method 1, we defined the rate of lesion enlargement as the difference in lesion size between the first and subsequent visit divided by the length of follow-up. As such, we referred to this method as the ALM, because it assumes a linear relationship between time and enlarging lesion area. The overall rate for the cohorts was calculated by performing a linear regression on individual patient rates, and the slope of the corresponding line was used as the rate of lesion enlargement. We calculated the rate of lesion enlargement for both SW-AF and NIR-AF imaging modalities in each of the two aforementioned patient groups (discrete and chorioretinal atrophy). The different rates of lesion enlargement were compared by using the analysis of covariance model. In addition, we explored the relationship between rate of lesion enlargement and baseline lesion size by calculating Pearson correlation coefficients (*r* values) between these two variables.

In Method 2, we defined rate of lesion enlargement by using the RLM as described by Shen et al.[25] This model proposes that the effective radius (the square root of [lesion area/π]) of lesions grows linearly with time, with the corresponding outcome measure being the rate of effective radius growth of the corresponding lesion area.[25] As performed in Method 1, we calculated the overall rate of effective radius growth by performing a linear regression on individual patient rates, and the slope of the corresponding line was taken as the rate of effective radius growth.

For both methods, we used Pearson correlation coefficients (*r* values) to analyze the relationship between rate of lesion enlargement and baseline lesion size. The statistical analyses, Bland-Altman plots, and linear regressions were performed using the GraphPad Prism 8 software (GraphPad Software, San Diego, CA, USA).

Results

The average age of the cohort was 33 ± 16 years (mean ± SD). Complete patient genotypes and age profile are summarized in the Supplementary Table.

Phenotypic Groups

Six patients (5%) were categorized as presenting with nascent atrophy (Fig. 1A). We defined nascent atrophy as early, atrophic changes confined to the macula, which presented as small, poorly delineated areas of hypoAF on SW-AF and NIR-AF images. The hypoAF areas appeared larger in NIR-AF images in all patients.

Twenty-one patients (18%) presented with widespread RPE atrophy (Fig. 1B). Widespread atrophy was defined as changes presenting with flecks throughout the posterior pole and with disease extending beyond the macula. Macular hypoAF was observed in both SW-AF and NIR-AF images, whereas the majority of flecks were hyperAF in SW-AF images and hypoAF in NIR-AF images. As with the nascent atrophy phenotype, hypoAF regions were larger in NIR-AF images.

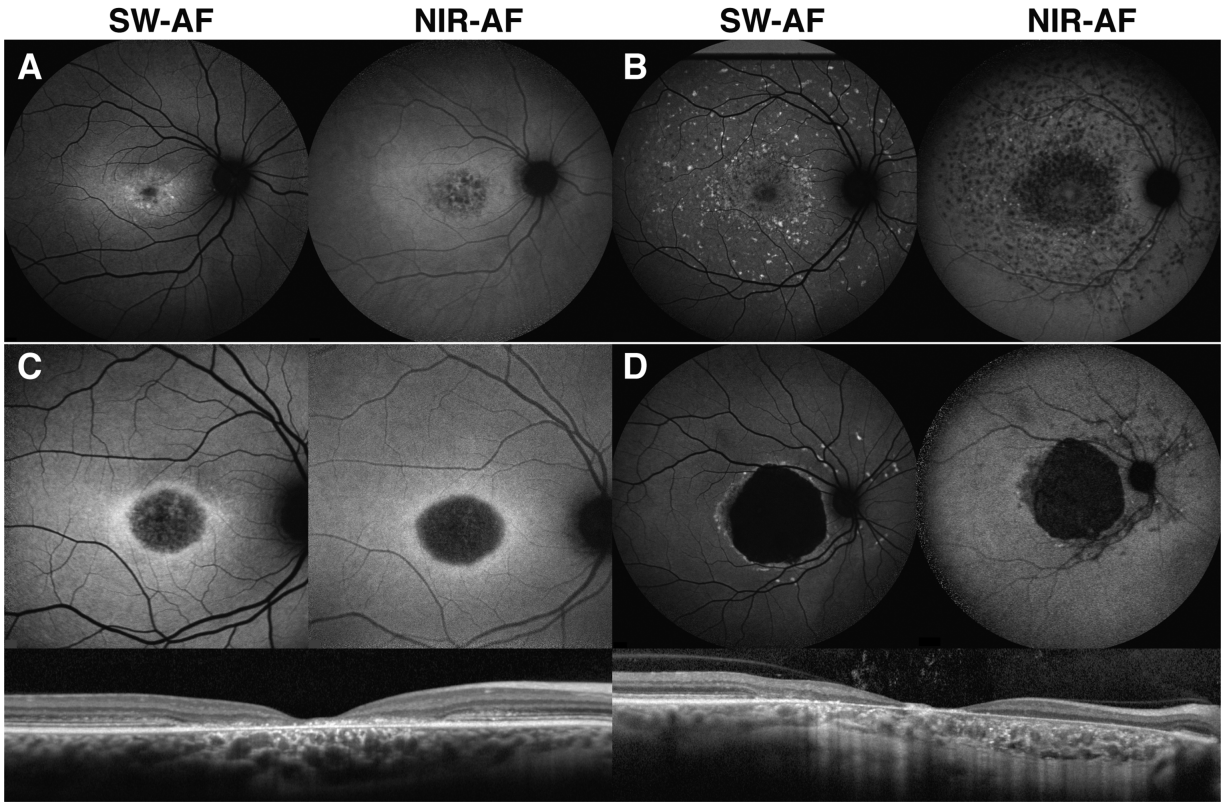

Figure 1. Phenotypes of recessive Stargardt disease in SW-AF and NIR-AF. (A) Patients characterized as presenting with nascent RPE atrophy exhibited early atrophic changes observed as small areas of hypoAF confined to the macula. (B) Patients that presented with widespread RPE atrophy phenotype exhibited disease that extended beyond the macula and throughout the posterior pole. Macular hypoAF was observed on both SW-AF and NIR-AF images, with the majority of flecks appearing as hyperAF on SW-AF images and hypoAF in NIR-AF images. (C) Patients that presented with the discrete RPE atrophy phenotype exhibited well-delineated areas of macular hypoAF in both SW-AF and NIR-AF images. On SD-OCT scans, fragmented remnants of the EZ band and collapse of the overlying retinal layers were visible in the lesion area. Transmission of the SD-OCT signal into the choroid was also observed, further suggestive of RPE atrophy. (D) Patients that presented with the chorioretinal RPE atrophy exhibited well-demarcated areas of hypoAF on SW-AF and NIR-AF images, with the intensity of the hypoAF comparable to that of the optic disk. On SD-OCT scans, complete disappearance of the outer retinal layers and thinned retina were observed, with a high level of signal transmission beyond the retina.

Fifty-five patients (48%) presented with discrete areas of RPE atrophy (Fig. 1C). Discrete atrophy presented as well-delineated, well-demarcated macular hypoAF areas in both SW-AF and NIR-AF images. In 33 patients, the hypoAF area was surrounded by a ring of hyperAF in both imaging modalities, whereas 22 patients either did not have a surrounding hyperAF ring ($n = 8$) or presented with a surrounding mottled ring of hyperAF intertwined with hypoAF ($n = 14$). In SD-OCT scans, fragmented remnants of the EZ band and collapse of the overlying retinal layers were visible in the lesion area. Transmission of the SD-OCT signal into the choroid was also observed, further suggestive of RPE atrophy.

Thirty-three patients (29%) presented with chorioretinal atrophy (Fig. 1D). We defined chorioretinal atrophy as well-demarcated areas of RPE atrophy, suggested by the dense hypoAF regions observed in SW-AF and NIR-AF images. The lack of AF signal in these areas was comparable to that observed at the optic disk, as opposed to patients with discrete atrophy, where the hypoAF areas were not as dark. In SD-OCT scans, chorioretinal atrophy was suggested by the complete disappearance of the outer retinal layers, collapse of the inner retinal layers, and an overall thinned retina in the atrophic areas. A higher level of signal transmission into the choroid was observed compared to patients with discrete atrophy. On fundoscopy, the underlying white sclera was visible in these areas of chorioretinal atrophy.

Lesion Areas and Rates of Enlargement

We measured the areas of macular hypoAF in discrete and chorioretinal patients (Fig. 2). In patients with discrete atrophy, we observed that the area of

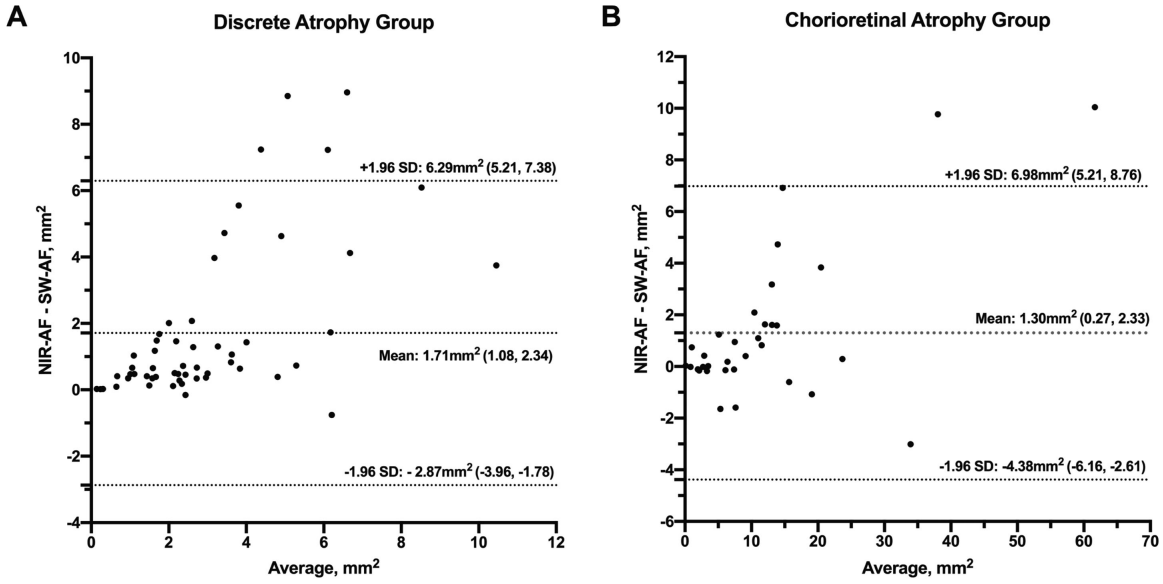

Figure 2. Bland-Altman plots showing the difference in size of the atrophic lesions in SW-AF and NIR-AF. For both patients with discrete (A) and chorioretinal atrophy (B), the size of the atrophic lesions appeared larger in NIR-AF images compared to SW-AF images. The numbers in parentheses represent the 95% confidence intervals for both the mean and the limits of agreement (±1.96 SD).

Table 2. Rates of Lesion Enlargement According to the Area Linear Model (Area Enlargement Rate) and Radius Linear Model (Effective Radius Enlargement Rate)

			Area Enlargement Rate (95% CI; mm²/y)			Effective Radius Enlargement Rate (95% CI; mm/y)		
Group	No.	Follow-up Length (yr)	SW-AF	NIR-AF	*P* Value*	SW-AF	NIR-AF	*P* Value*
Discrete	29	2.7 ± 1.8	0.20 (0.05–0.35)	0.32 (0.15–0.49)	0.275	0.03 (0.01–0.05)	0.05 (0.03–0.07)	0.221
Chorioretinal	21	2.6 ± 1.6	1.30 (0.06–2.6)	1.74 (0.03–3.4)	0.671	0.08 (0.02–0.09)	0.10 (0.03–0.09)	0.754

Rates are reported for both SW-AF and NIR-AF imaging for patients in the discrete and chorioretinal groups. Data are summarized as mean ± SD where applicable.

**P*-value calculated by the analysis of covariance model.

atrophy was greater in NIR-AF images than in SW-AF images (3.9 ± 0.4 mm² vs. 2.2 ± 0.2 mm², $P < 0.001$). Similarly, in patients with chorioretinal atrophy, the atrophic areas were greater in NIR-AF (12.7 ± 2.4 mm²) as compared to SW-AF images (11.4 ± 2.1 mm², $P = 0.015$).

Imaging from a follow-up visit was available for 29 patients in the discrete group (average follow-up time: 2.7 ± 1.8 years) and 21 patients in the chorioretinal group (average follow-up time: 2.6 ± 1.6 years), where we observed disease progression (Fig. 3). We calculated rates of lesion enlargement for these patients using linear regressions with both the ALM and RLM models (Fig. 4). When using the ALM, we observed an area enlargement rate of 0.20 mm²/y (95% confidence interval [CI]: 0.05–0.35) in SW-AF and 0.32 mm²/y (95% CI: 0.15–0.49) in NIR-AF images ($P = 0.275$) in the discrete group, whereas this rate was 1.30 mm²/y (95% CI: 0.06–2.60) in SW-AF and 1.74 mm²/y (95% CI: 0.03–3.44) in NIR-AF images ($P = 0.671$) in the chorioretinal atrophy group (Figs. 4A, 4B) . When using the RLM model, we observed an effective radius enlargement rate of 0.03 mm²/y (95% CI: 0.01–0.05) in SW-AF and 0.05 mm²/y (95% CI: 0.03–0.07) in NIR-AF images ($P = 0.221$) in the discrete group, whereas this rate was 0.08 mm²/y (95% CI: 0.02–0.09) on SW-AF and 0.10 mm²/y (95% CI: 0.03–0.09) in NIR-AF images ($P = 0.754$) from the chorioretinal group (Figs. 4C, 4D). These results are summarized in Table 2.

We also compared the enlargement rates from each imaging modality in the two phenotypes. Using the ALM model, we observed a faster rate of enlargement in the chorioretinal atrophy group (SW-AF:

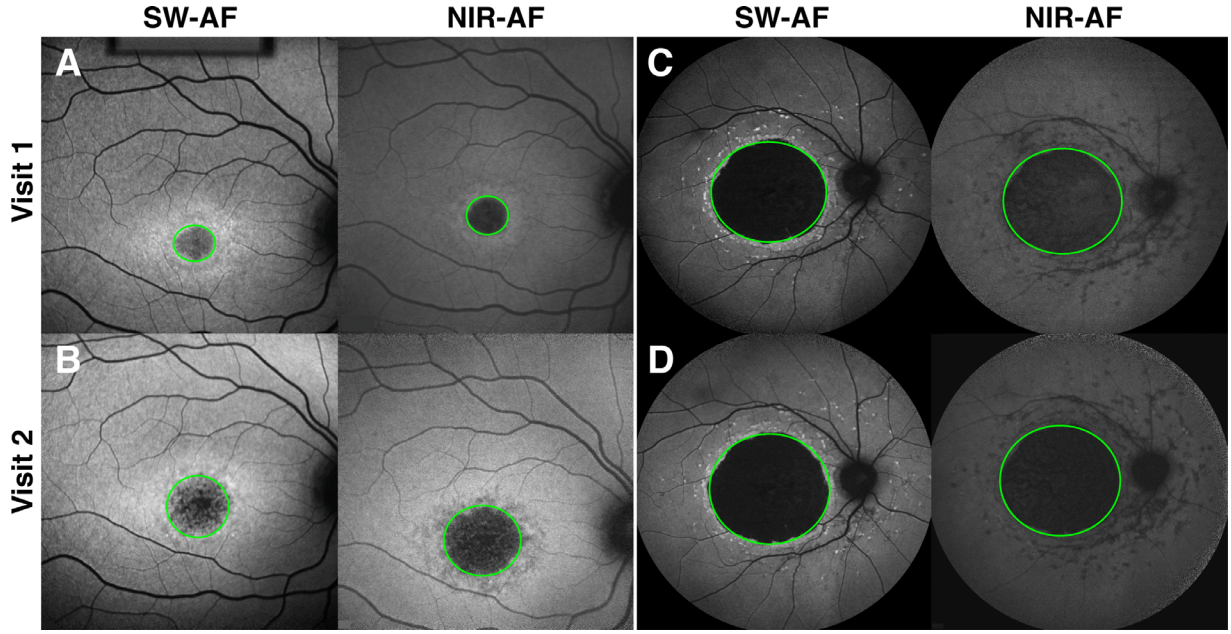

Figure 3. Progression of recessive Stargardt disease in SW-AF and NIR-AF. Patient 10 (A, B) presented with a phenotype showing discrete RPE atrophy at presentation (visit 1, A). On a follow-up visit five years later (visit 2, B), the areas of atrophy had increased in size in both SW-AF and NIR-AF images. Patient 46 (C, D) exhibited a phenotype of chorioretinal atrophy at visit 1 (C) and visit 2 (D) five years later, with the atrophic lesions also increasing in size between the two visits. The measured areas of atrophy are delineated in green.

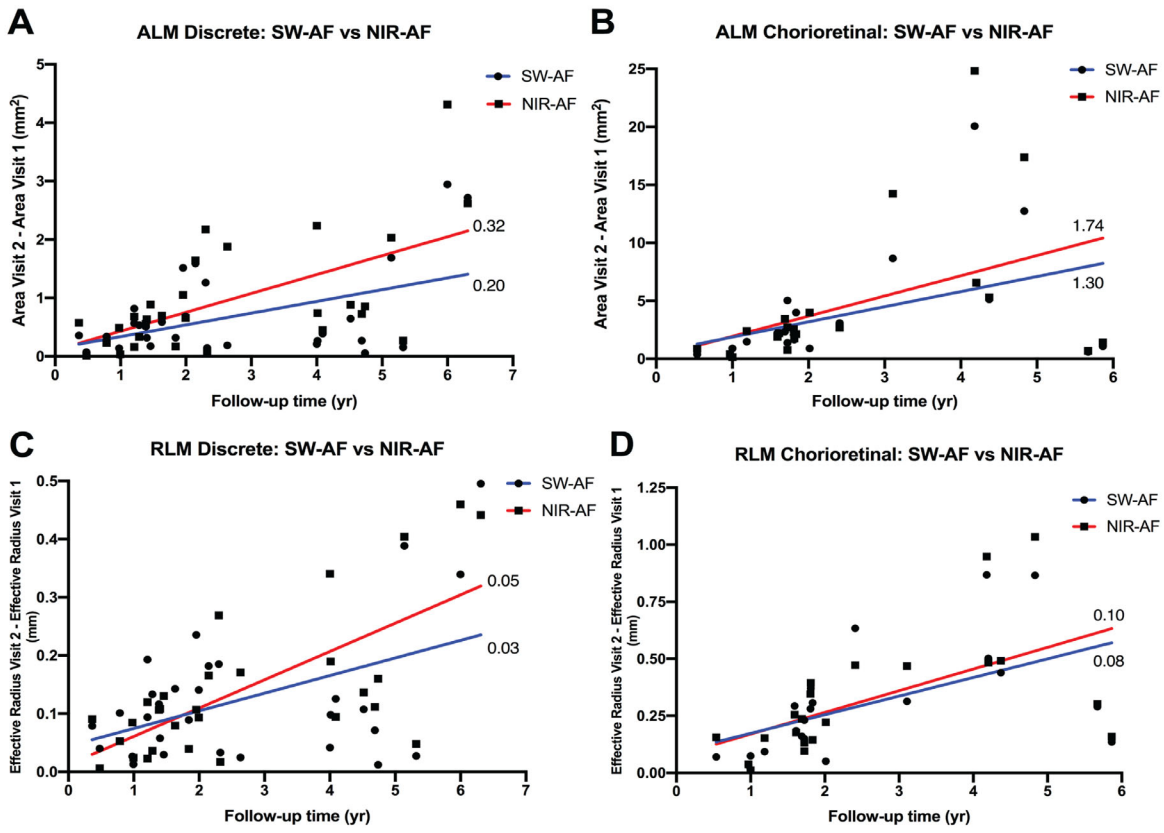

Figure 4. Rates of lesion enlargement calculated from linear regressions. The graphs demonstrate linear regressions for calculating the rate of lesion enlargement observed on SW-AF and NIR-AF images with the area linear model for discrete atrophy (A) and chorioretinal atrophy (B) patients. Similar graphs for rates calculated with the radius linear model are presented for patients with discrete (C) and chorioretinal atrophy (D).

1.30 mm^2/y; NIR-AF: 1.74 mm^2/y) compared to the discrete atrophy group (SW-AF: 0.20 mm^2/y; NIR-AF: 0.32 mm^2/y) in both SW-AF ($P = 0.036$) and NIR-AF ($P = 0.039$) images. In the RLM model, however, similar rates of enlargement were observed in the chorioretinal atrophy group (SW-AF: 0.08 mm/y; NIR-AF: 0.10 mm/y) compared to the discrete atrophy group (SW-AF: 0.03 mm/y; NIR-AF: 0.05 mm/y) in both SW-AF ($P = 0.069$) and NIR-AF ($P = 0.106$) images.

We analyzed the correlation between baseline lesion size and rates of lesion enlargement. We observed a significant correlation between the ALM rates of enlargement and baseline lesion size in chorioretinal atrophy patients (SW-AF: $r = 0.655$, $P = 0.001$; NIR-AF: $r = 0.774$, $P < 0.001$). In patients with discrete atrophy, however, a significant correlation was only observed in enlargement rates obtained from NIR-AF images ($r = 0.424$, $P = 0.022$), as opposed to rates obtained from SW-AF images ($r = 0.262$, $P = 0.169$). When analyzing the enlargement rates obtained using the RLM, no significant correlation with baseline lesion size was observed in patients with discrete atrophy (SW-AF: $r = -0.083$, $P = 0.668$; NIR-AF: $r = 0.179$, $P = 0.350$) or in patients with chorioretinal atrophy (SW-AF: $r = -0.157$, $P = 0.496$; NIR-AF: $r = -0.035$, $P = 0.881$) for either imaging modality.

Discussion

We analyzed a large cohort of STGD1 patients and compared the extent of RPE atrophy in SW-AF and NIR-AF images. From both our qualitative and quantitative analyses, we observed that hypoAF areas appear larger in NIR-AF images. This is clearly observed, for example, in patients with nascent (Fig. 1A) and widespread (Fig. 1B) atrophy. Similarly, when we quantitatively analyzed the patients with discrete and chorioretinal atrophy, we also observed that the lesions appeared greater in NIR-AF images. Our results from this study with a large patient cohort (115 eyes from 115 patients) are in accordance with previous studies reporting analyses of both imaging modalities in smaller cohorts of STGD1 patients.[13–15] For example, two earlier publications from our group, Greenstein et al.[13] (15 eyes from 15 patients) and Duncker et al.[14] (45 eyes from 24 patients), also demonstrated in that the areas of atrophy in NIR-AF images are larger than those observed in SW-AF images. Of note, the cohort in this present study contains 13 patients from the study by Greenstein et al.[13] and 19 patients from the study by Duncker et al.[14] study, with 13 patients present in all three studies. Based on qualitative assessment, Kellner et al.[15] observed similar findings in a cohort of 16 patients. In a recent prospective study of 44 patients (88 eyes), Muller et al.[16] studied AF abnormalities by measuring their eccentricity along a foveopapillary trajectory, rather than measuring the area, and found larger abnormalities in NIR-AF images. More recently, a study by Cicinelli et al.[26] (54 eyes from 28 patients) reported that rates of RPE atrophy obtained from SW-AF and NIR-AF images are similar, but that the agreement decreased as the rate increased. As compared to these previous studies, the strength of ours is not only the much larger cohort size (115 eyes from 115 patients), but also the analysis based on phenotypic presentation and the calculations of lesion enlargement rates with two different models (ALM, RLM).

As described previously, ALM assumes a linear relationship between time and enlarging lesion area, and it has been used widely in multiple studies to characterize lesion enlargement in STGD1, including the ProgStar studies designed to characterize the natural history of STGD1.[21,22,27–31] Using this model, we observed similar rates of lesion enlargement between SW-AF and NIR-AF images in each of the discrete and chorioretinal group. Nevertheless, the rates observed for both imaging modalities were faster in the chorioretinal group compared to the discrete. These results suggest that STGD1 progresses differently based on phenotype and/or disease stage, which has been suggested by previous studies by Fujinami et al.[28] and Cicinelli et al.,[26] albeit both with different phenotypic characterizations to ours. In the ProgStar studies, hypoAF areas defined as "definitely decreased autofluorescence (DDAF)" roughly correspond to the chorioretinal atrophy grouping in the current study, whereas "questionable decreased autofluorescence (QDAF)" correspond to the areas we refer to as discrete.[21,22] The investigators conducting the prospective study reported that areas of DDAF increased by 0.76 mm^2/y, whereas the total area of decreased AF, the sum of the DDAF and QDAF areas, increased by 0.64 mm^2/y.[21] Based on a retrospective study, the rates were also reported to increase by 0.51 mm^2/y for DDAF and 0.35 mm^2/y for total area of decreased AF.[22] Nevertheless, a weakness of the ALM is that the calculated rates of enlargement are dependent on the size of the baseline lesion as previously described.[25] We also observed that our enlargement rates from both imaging modalities correlate with baseline lesion size in the chorioretinal atrophy group, whereas only the enlargement rate from NIR-AF images correlated with baseline lesion size in the discrete group. As such, given that the baseline lesion sizes were larger in the

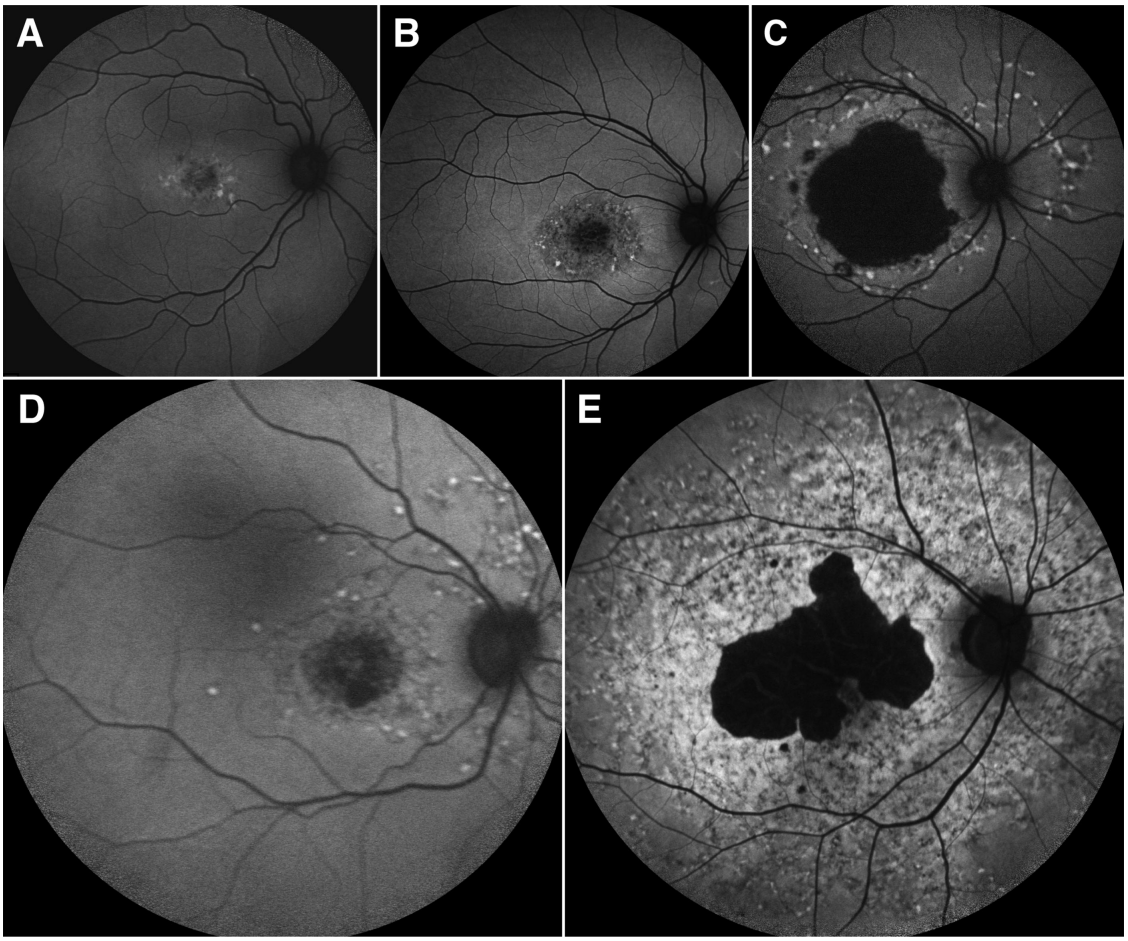

Figure 5. Role of genotype, age, and other potential factors in the presenting phenotype of recessive Stargardt disease. Patient 78 (28 years old, A), Patient 43 (30 years old, B), and Patient 98 (62 years old, C) all presented with recessive Stargardt disease caused by the variants c.3050+5G>A and p.G1961E. Patient 98 presented with a chorioretinal phenotype of RPE atrophy, suggestive of more advanced disease, whereas both Patients 78 and 43 presented with a less-severe discrete phenotype of RPE atrophy. Similarly, Patient 68 (72 years old, D) and Patient 70 (76 years old, E) are both of similar age and both carry the pathogenic variants p.D1532N and p.G1961E, yet Patient 70 presented with a more advanced phenotype. These images suggest that the presenting phenotype of recessive Stargardt disease is influenced by genotype, age, and other potential factors such as environmental.

chorioretinal group compared to the discrete group (SW-AF: 11.4 mm^2, NIR-AF: 12.7 mm^2 vs. SW-AF: 2.2 mm^2, NIR-AF: 3.9 mm^2), we considered this difference in baseline lesion size to be a confounding factor in the calculation of ALM rates and could explain why faster enlargement rates in the chorioretinal atrophy group were observed.

As opposed to the ALM, the lesion enlargement rates obtained using the RLM model have been shown to be independent of baseline lesion size.[25] When we reanalyzed this relationship in the current study, we also did not find a significant correlation for either imaging modality in either the chorioretinal or discrete atrophy groups. Similar to the ALM, we observed similar enlargement rates in SW-AF and NIR-AF images for both the discrete and chorioretinal groups. Unlike the ALM, however, we did not observe a difference in enlargement rates between discrete and chorioretinal atrophy groups. As we hypothesized earlier, the difference in rates observed with the ALM was likely due to the difference in baseline lesion size between the two groups. The rates we obtained using the RLM approach are similar to those reported by Shen et al.[25] (0.104 mm/y; 95% CI: 0.086–0.123 mm/y).

Through analyses of the discrete and chorioretinal phenotypes with multiple imaging modalities, we can conclude that disease is more severe in the chorioretinal phenotype. On AF images, for example, the apparent darker hypoAF areas suggest a greater degree of RPE atrophy. This observation is further suggested when we examine SD-OCT scans, where the outer retinal layers are completely atrophied in chorioretinal patients and

sub-RPE hypertransmission of OCT signal is more pronounced (Figs. 1C, 1D). Furthermore, in a previous study from our group, we observed more significant atrophy of the choriocapillaris as detected by OCT angiography in patients with chorioretinal atrophy compared to patients with discrete atrophy.[32] Despite the difference in disease severity between these two phenotypes, however, we observed a similar rate of lesion enlargement between the two groups, suggesting that the process of RPE atrophy is similar amongst different STGD1 phenotypes.

Although we describe four phenotypic groups in this study, we acknowledge that the clinical phenotype is just a snapshot of the patient's disease at a given time. Moreover, a particular less-severe phenotype could advance to a more severe phenotype based on the patient's age, genotype, and other uncharacterized genetic/environmental factors. For example, a large portion of patients with the nascent and discrete phenotypes harbored the p.(G1961E) variant (83% and 45%, respectively, Table 1), indicating that this variant is typically associated with a disease form confined to the macula. Previous studies have similarly reported that fundus changes associated with this variant tend to localize to the foveal and parafoveal area.[33–35] Furthermore, patients 43, 78, and 98 in Figures 5A to 5C all had the same genotype; they were compound heterozygous for the c.3050+5G>A and p.(G1961E) variants. Patients 78 and 43 were 28 and 30 years old, respectively, and both had a phenotype of discrete RPE atrophy, whereas patient 98, a 62-year-old, also had the same genotype, but phenotypically his disease was more severe because he exhibits chorioretinal atrophy. This would suggest that as these patients age, their phenotype progresses from discrete RPE atrophy to chorioretinal atrophy. The patients with chorioretinal atrophy in our study were indeed generally older as compared to the patients in other groups (Table 1). Similarly, patients 68 and 70 were compound heterozygous for the p.(D1532N) and p.(G1961E) variants and were of similar age (72 and 76 years, respectively), but patient 68 presented with widespread RPE atrophy whereas patient 70 exhibited the more severe chorioretinal atrophy (Figs. 5D, 5E). This difference may indicate that other factors such as the environment or modifier genes in addition to age and genotype are involved in determining the phenotype.

Our study presents with some limitations. Because we conducted measurements and reported rates of lesion enlargement with units of either mm^2 in the ALM or mm in the RLM, we are aware that there is uncertainty in the absolute magnitude of these measurements and rates because of individual differences in axial length between individual subjects that the measuring software does not account for. Furthermore, we acknowledge that a patient can progress from one phenotype to another, although this was not observed in any of the patients from this study.

In conclusion, we used two different models to analyze the rates of lesion enlargement in both SW-AF and NIR-AF imaging. When comparing the two models, we found it to be more advantageous to use the RLM due to its independence from baseline lesion size. We also did not observe a significant difference in the rates of lesion enlargement obtained from SW-AF and NIR-AF images for either model of analysis. This finding suggests that although the areas of RPE atrophy appear larger in NIR-AF images, the underlying process of atrophy progression is detected similarly by both imaging modalities. Furthermore, NIR-AF imaging confers other important advantages over SW-AF. Given that NIR-AF images detect a larger area of RPE atrophy, NIR-AF imaging may be superior in detecting lesions that are missed by SW-AF images in patients with an early disease stage. Additionally, there have been concerns regarding the frequent use of SW-AF imaging.[36] As such, NIR-AF imaging confers important advantages that warrant a more frequent use in the monitoring of STGD1 patients.

Acknowledgments

Supported by the National Institutes of Health grants [R01 EY024091, R01 EY029315]; Foundation Fighting Blindness awards [TA-NMT-0116-0692-COLU and PPA-1218-0751-COLU]; and unrestricted grant from Research to Prevent Blindness (RPB) to the Department of Ophthalmology, Columbia University, New York, NY, USA.

Disclosure: **R. Jauregui,** None; **Y. Nuzbrokh,** None; **P.-Y. Su,** None; **J. Zernant,** None; **R. Allikmets,** None; **S.H. Tsang,** None; **J.R. Sparrow,** None

References

1. Fishman GA, Farber M, Patel BS, Derlacki DJ. Visual acuity loss in patients with Stargardt's macular dystrophy. *Ophthalmology.* 1987;94(7):809–814.
2. Rotenstreich Y, Fishman GA, Anderson RJ. Visual acuity loss and clinical observations in a large series of patients with Stargardt disease. *Ophthalmology.* 2003;110(6):1151–1158.

3. Allikmets R, Singh N, Sun H, et al. A photoreceptor cell-specific ATP-binding transporter gene (ABCR) is mutated in recessive Stargardt macular dystrophy. *Nat Genet.* 1997;15(3):236–246.
4. Quazi F, Molday RS. ATP-binding cassette transporter ABCA4 and chemical isomerization protect photoreceptor cells from the toxic accumulation of excess 11-cis-retinal. *Proc Natl Acad Sci USA.* 2014;111(13):5024–5029.
5. Weng J, Mata NL, Azarian SM, Tzekov RT, Birch DG, Travis GH. Insights into the function of Rim protein in photoreceptors and etiology of Stargardt's disease from the phenotype in abcr knockout mice. *Cell.* 1999;98(1):13–23.
6. Cideciyan AV, Aleman TS, Swider M, et al. Mutations in ABCA4 result in accumulation of lipofuscin before slowing of the retinoid cycle: a reappraisal of the human disease sequence. *Hum Mol Genet.* 2004;13(5):525–534.
7. Burke TR, Duncker T, Woods RL, et al. Quantitative fundus autofluorescence in recessive Stargardt disease. *Invest Ophthalmol Vis Sci.* 2014;55(5):2841–2852.
8. Walia S, Fishman GA, Kapur R. Flecked-retina syndromes. *Ophthalmic Genet.* 2009;30(2):69–75.
9. Sparrow JR, Marsiglia M, Allikmets R, et al. Flecks in recessive Stargardt disease: short-wavelength autofluorescence, near-infrared autofluorescence, and optical coherence tomography. *Invest Ophthalmol Vis Sci.* 2015;56(8):5029–5039.
10. Delori FC, Dorey CK, Staurenghi G, Arend O, Goger DG, Weiter JJ. In vivo fluorescence of the ocular fundus exhibits retinal pigment epithelium lipofuscin characteristics. *Invest Ophthalmol Vis Sci.* 1995;36(3):718–729.
11. Paavo M, Lee W, Allikmets R, Tsang S, Sparrow JR. Photoreceptor cells as a source of fundus autofluorescence in recessive Stargardt disease. *J Neurosci Res.* 2019;97(1):98–106.
12. Keilhauer CN, Delori FC. Near-infrared autofluorescence imaging of the fundus: visualization of ocular melanin. *Invest Ophthalmol Vis Sci.* 2006;47(8):3556–3564.
13. Greenstein VC, Schuman AD, Lee W, et al. Near-infrared autofluorescence: its relationship to short-wavelength autofluorescence and optical coherence tomography in recessive Stargardt disease. *Invest Ophthalmol Vis Sci.* 2015;56(5):3226–3234.
14. Duncker T, Marsiglia M, Lee W, et al. Correlations among near-infrared and short-wavelength autofluorescence and spectral-domain optical coherence tomography in recessive Stargardt disease. *Invest Ophthalmol Vis Sci.* 2014;55(12):8134–8143.
15. Kellner S, Kellner U, Weber BH, Fiebig B, Weinitz S, Ruether K. Lipofuscin- and melanin-related fundus autofluorescence in patients with ABCA4-associated retinal dystrophies. *Am J Ophthalmol.* 2009;147(5):895–902.e891.
16. Muller PL, Birtel J, Herrmann P, Holz FG, Charbel Issa P, Gliem M. Functional relevance and structural correlates of near infrared and short wavelength fundus autofluorescence imaging in ABCA4-related retinopathy. *Transl Vis Sci Technol.* 2019;8(6):46.
17. Duncker T, Tabacaru MR, Lee W, Tsang SH, Sparrow JR, Greenstein VC. Comparison of near-infrared and short-wavelength autofluorescence in retinitis pigmentosa. *Invest Ophthalmol Vis Sci.* 2013;54(1):585–591.
18. Jauregui R, Park KS, Duong JK, Sparrow JR, Tsang SH. Quantitative comparison of near-infrared versus short-wave autofluorescence imaging in monitoring progression of retinitis pigmentosa. *Am J Ophthalmol.* 2018;194:120–125.
19. Wolock CJ, Stong N, Ma CJ, et al. A case-control collapsing analysis identifies retinal dystrophy genes associated with ophthalmic disease in patients with no pathogenic ABCA4 variants. *Genet Med.* 2019;21(10):2336–2344.
20. Kalia SS, Adelman K, Bale SJ, et al. Recommendations for reporting of secondary findings in clinical exome and genome sequencing, 2016 update (ACMG SF v2.0): a policy statement of the American College of Medical Genetics and Genomics. *Genet Med.* 2017;19(2):249–255.
21. Strauss RW, Kong X, Ho A, et al. Progression of Stargardt disease as determined by fundus autofluorescence over a 12-month period: ProgStar Report No. 11. *JAMA Ophthalmol.* 2019;137(10):1134–1145.
22. Strauss RW, Munoz B, Ho A, et al. Progression of Stargardt disease as determined by fundus autofluorescence in the retrospective progression of Stargardt Disease Study (ProgStar Report No. 9). *JAMA Ophthalmol.* 2017;135(11):1232–1241.
23. Panthier C, Querques G, Puche N, et al. Evaluation of semiautomated measurement of geographic atrophy in age-related macular degeneration by fundus autofluorescence in clinical setting. *Retina.* 2014;34(3):576–582.
24. Schmitz-Valckenberg S, Brinkmann CK, Alten F, et al. Semiautomated image processing method for identification and quantification of geographic atrophy in age-related macular degeneration. *Invest Ophthalmol Vis Sci.* 2011;52(10):7640–7646.
25. Shen LL, Sun M, Grossetta Nardini HK, Del Priore LV. Natural history of autosomal recessive

stargardt disease in untreated eyes: a systematic review and meta-analysis of study- and individual-level data. *Ophthalmology.* 2019;126(9):1288–1296.
26. Cicinelli MV, Rabiolo A, Brambati M, Vigano C, Bandello F, Battaglia Parodi M. Factors influencing retinal pigment epithelium-atrophy progression rate in Stargardt disease. *Transl Vis Sci Technol.* 2020;9(7):33.
27. Di Iorio V, Orrico A, Esposito G, et al. Association between genotype and disease progression in Italian Stargardt patients: a retrospective natural history study. *Retina.* 2019;39(7):1399–1409.
28. Fujinami K, Lois N, Mukherjee R, et al. A longitudinal study of Stargardt disease: quantitative assessment of fundus autofluorescence, progression, and genotype correlations. *Invest Ophthalmol Vis Sci.* 2013;54(13):8181–8190.
29. Kong X, West SK, Strauss RW, et al. Progression of visual acuity and fundus autofluorescence in recent-onset Stargardt disease: ProgStar Study Report #4. *Ophthalmol Retina.* 2017;1(6):514–523.
30. Chen B, Tosha C, Gorin MB, Nusinowitz S. Analysis of autofluorescent retinal images and measurement of atrophic lesion growth in Stargardt disease. *Exp Eye Res.* 2010;91(2):143–152.
31. McBain VA, Townend J, Lois N. Progression of retinal pigment epithelial atrophy in stargardt disease. *Am J Ophthalmol.* 2012;154(1):146–154.
32. Jauregui R, Cho A, Lee W, et al. Progressive choriocapillaris impairment in ABCA4 maculopathy is secondary to retinal pigment epithelium atrophy. *Invest Ophthalmol Vis Sci.* 2020;61(4):13.
33. Genead MA, Fishman GA, Stone EM, Allikmets R. The natural history of Stargardt disease with specific sequence mutation in the ABCA4 gene. *Invest Ophthalmol Vis Sci.* 2009;50(12):5867–5871.
34. Cella W, Greenstein VC, Zernant-Rajang J, et al. G1961E mutant allele in the Stargardt disease gene ABCA4 causes bull's eye maculopathy. *Exp Eye Res.* 2009;89(1):16–24.
35. Burke TR, Fishman GA, Zernant J, et al. Retinal phenotypes in patients homozygous for the G1961E mutation in the ABCA4 gene. *Invest Ophthalmol Vis Sci.* 2012;53(8):4458–4467.
36. Cideciyan AV, Swider M, Aleman TS, et al. Reduced-illuminance autofluorescence imaging in ABCA4-associated retinal degenerations. *J Opt Soc Am A Opt Image Sci Vis.* 2007;24(5):1457–1467.